JOURNAL OF MATERIALS SCIENCE 37 (2002) 5183–5189

Characterization of dispersed intermetallic phases in an Al-8.32wt%Fe-3.4wt%Ce alloy

L. C. ZHANG*,§,¶, A. Q. HE*, H. Q. YE*, C. HUANG‡, Y. C. ZHANG‡
*Laboratories of *Atomic Imaging of Solids and ‡Microcrystal, Institute of Metal Research, Chinese Academy of Sciences, Shenyang 110015, People's Republic of China*
E-mail: lxz29@po.cwru.edu

A rapidly solidified Al-8.32Fe-3.4Ce (wt%) alloy was prepared by gas atomization and extrusion. The intermetallic phases present and their thermal stability, at temperatures up to 400°C, have been investigated by means of transmission electron microscopy (TEM). The metastable Al_mFe, Al_8Ce and equilibrium $Al_{13}Fe_4$ phases were detected in the as-extruded sample and the sample heat-exposed at 230°C, whereas the equilibrium $Al_{13}Fe_4$ and $Al_{13}Fe_3Ce$ phases existed in the samples heat-exposed at temperatures above 315°C. The Al_mFe and the Al_8Ce phases were firstly observed in this alloy. The $Al_{10}Fe_2Ce$ and $Al_{20}Fe_5Ce$ phases, which were reported by the others in the similar alloys, do not exist in our samples. In addition, various domain structures in $Al_{13}Fe_3Ce$ were also studied.

1. Introduction

Generally, the dispersed intermetallic phases occupy a volume fraction of 25–30% in a rapidly solidified (RS) Al-Fe-Ce alloy. These phases distribute homogeneously in the α-Al solid solution and grain boundaries, and play an important strengthening role at high temperature. Precipitation of these phases in the RS Al-Fe-Ce alloy is very complicated. This precipitation process was so far investigated in a few literatures [1–3]. However, there exist some discrepancies among these reports. Angers [1] detected five dispersed phases in as-extruded RS Al-8.8Fe-3.7Ce and Al-8.9Fe-6.9Ce(wt%) alloys, which are metastable Al_6Fe, two metastable Al-Fe-Ce phases, and two equilibrium phases α-$Al_{13}Fe_4$ and $Al_{10}Fe_2Ce$; Ayer *et al*. [2] reported that there exist metastable Al_6Fe, $Al_{10}Fe_2Ce$, quasicrystal $Al_{20}Fe_5Ce$ phases, and the equilibrium α-$Al_{13}Fe_4$ and $Al_{13}Fe_3Ce$ phases in a RS Al-8.8Fe-3.7Ce alloy. Grleb [3] reexamined the Al-Fe-Ce phase diagram and pointed out that the $Al_{20}Fe_5Ce$ and $Al_{13}Fe_3Ce$ were not equilibrium phases. The reasons for these discrepancies may be related to different solidification processes employed to produce the Al-Fe-Ce alloys. In spite of some differences, the metastable Al_mFe and Al_8Ce phases, which will be shown in this paper, were never reported in these literatures [1–3]. In this paper, we will study these present phases as well as thermal stability of these phases in a RS Al-8.32Fe-3.4Ce (wt%) alloy.

2. Experimental procedure

The alloy, with nominal composition (wt%) of Al-8.32Fe-3.4Ce, was prepared by gas atomization, followed by vacuum hot extrusion. The extrusion temperature is 400°C. Most samples were heat exposed at 230°C for 100 hours, 315°C for 100 hours, 400°C for 30 and 70 hours, respectively. The TEM foils were obtained by two-jet electro-polishing in an electrolyte containing one part HNO_3 and three-part CH_3OH (by volume), and then ion milling. JEM-200CX transmission electron microscopy (TEM) with large angle tilting holder was employed to identify the morphologies and structures of the intermetallic phases. High-resolution TEM was performed in a JEM-2000EX(II) with ultra-high resolution pole pieces to examine defect and interfacial structures in the intermetallic phases.

3. Results and discussion

3.1. Microstructure

The morphologies of the samples are shown in Fig. 1. Fig. 1a was taken from the as-extruded sample and Fig. 1b from the one heat-exposed at 230°C for 100 hrs. Fig. 1a and b clearly show that the morphologies of these two samples are basically similar, all consisting of fine precipitates (M zone) and relatively large intermetallic compounds (C zone). Fig. 1c and d were taken from the samples heat-exposed at 315°C for 100 hrs and 400°C for 100 hrs, respectively. In comparison with Fig. 1a and b, the intermetallic phases in Fig. 1c and d become much coarser after heat exposure above 315°C. Jones *et al*. [4] pointed out that the microstructure with fine precipitates possesses a higher hardness value than that with coarse ones. From our earlier work [5], it is known that both tensile yield strength and hardness decrease slowly and the ductility increase a little when the heat exposure temperature is lower than 300°C in this

§Author to whom all correspondence should be addressed.
¶*Present Address*: Department of Materials Science and Engineering, Case Western Reserve University, Euclid 10900, Cleveland, OH44106, USA.

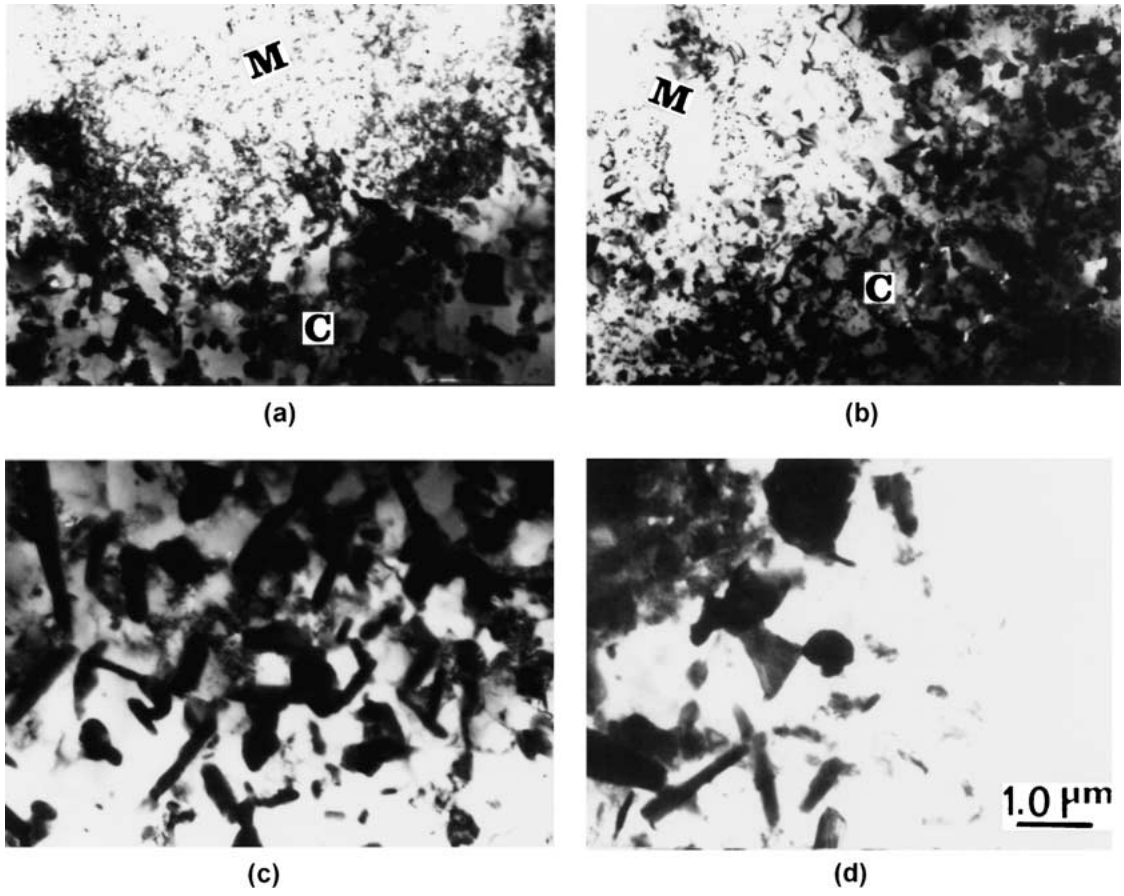

Figure 1 Typical morphologies in (a) the as-extruded sample, (b) the sample heat-exposed at 230°C for 100 hrs, (c) the sample heat-exposed at 315°C for 100 hrs, and (d) the sample heat-exposed at 400°C for 70 hrs.

TABLE I Intermetallic phases observed in various specimens with different heat treatment

Heat treatment	Intermetallic phases
As-extruded	α-Al, Al_8Ce, Al_mFe, α-$Al_{13}Fe_4$
230°C/100 hrs	α-Al, Al_8Ce, Al_mFe, α-$Al_{13}Fe_4$
315°C/100 hrs	Al_mFe, minor Al_8Ce, $Al_{16}Fe_3Ce$, α-$Al_{13}Fe_4$, $Al_{13}Fe_3Ce$
400°C/30 hrs	α-$Al_{13}Fe_4$, $Al_{13}Fe_3Ce$
400°C/100 hrs	α-$Al_{13}Fe_4$, $Al_{13}Fe_3Ce$

alloy; however, these properties degrade quickly when the heat exposure temperatures are higher than 300°C. According to our present TEM observation, this is consistent with the Jone's view [4].

Based on numerous TEM determinations, the intermetallic phases are summarized in Table I. Types of the phases are different with various heat exposure temperatures. In as-extruded state, the α-Al solid solution is highly supersaturated with Fe and Ce elements and some phases are thermal unstable, so transformation from the metastable to equilibrium phases occurs during heat exposure. When annealing the alloys below 300°C, the equilibrium phases were very difficult to nucleate and grow due to limited atomic diffusion coefficient; however, the equilibrium phases can grow relatively quickly due to the increased diffusion when annealing the alloys above 300°C. In detail from Table I, the Al_mFe and Al_8Ce phases should be the main strengthening phases in the samples heat exposed below 315°C, and the phase transformation must occur above 315°C since the Al_mFe and Al_8Ce phases do not exist any longer at the heat-exposure temperatures higher than 315°C.

It is noteworthy that types of the intermetallic phases show differences between our study and the others [1–3]. In our study, the metastable Al_mFe, Al_8Ce and $Al_{16}Ce_3Fe$ phases, the equilibrium α-$Al_{13}Fe_4$ and $Al_{13}Fe_3Ce$ phases were observed. In contrast with the previous results of Angers [1] and Ayer *et al*. [2], we never detected the Al_6Fe, $Al_{10}Fe_2Ce$ and $Al_{20}Fe_5Ce$ phases. These differences may result from various cooling rates during solidification. Skjerpe *et al*. [6] reported that metastable phases Al_mFe, Al_xFe, Al_9Fe_2 and the equilibrium phase α-$Al_{13}Fe_4$ could form in an Al-25Fe-13Si(wt%) alloy, and which one of these phases appeared depended on the alloy composition and the cooling rate during solidification. The equilibrium phase α-$Al_{13}Fe_4$ can form at a relatively low cooling rate, whereas the metastable Al-Fe-(Si) phases can form at a high cooling rate. Young *et al*.[7] studied the binary Al-Fe system, and observed $Al_{13}Fe_4$ only at a low cooling rate, while Al_xFe, Al_6Fe, Al_mFe and Al_9Fe_2 appeared in the sequence with increasing the cooling rates during solidification. This can be used to interpret our present results: Our alloys were prepared by the supersonic gas atomization technique with a relatively high cooling rate, so the metastable Al-Fe phase in this alloy could be Al_mFe, not Al_6Fe which was early reported in the literatures [1, 2]. Similarly, it is reasonable that

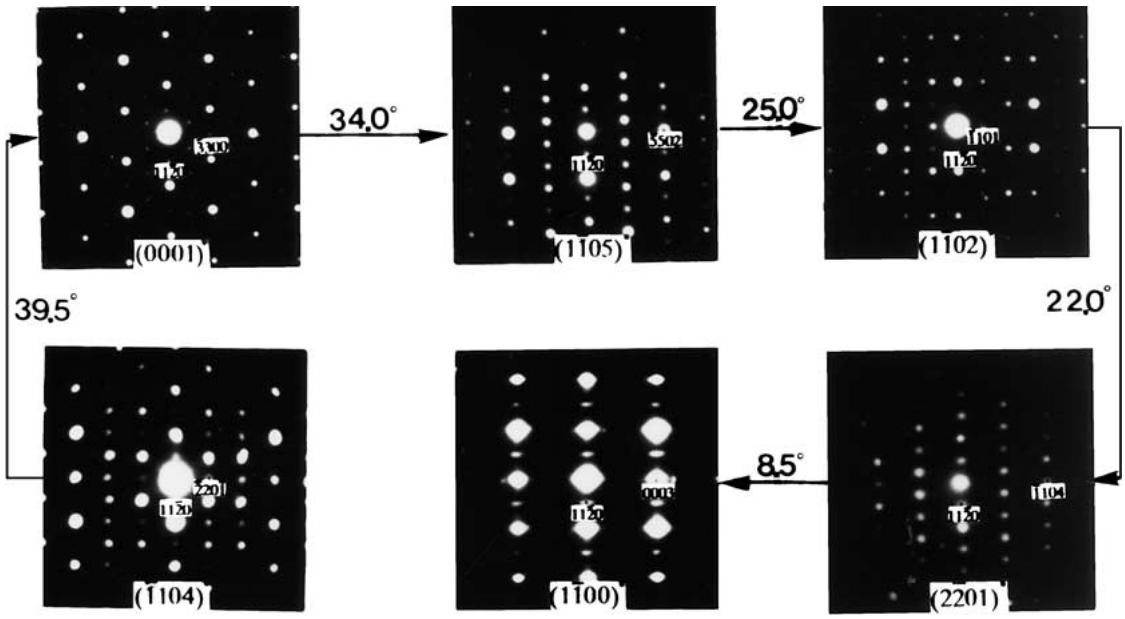

Figure 2 A series of DPs which were taken from Al_8Ce around the [11–20]* reciprocal axis.

the relatively high cooling rate be also responsible for formation of the metastable phase Al_8Ce newly found in this alloy.

In addition, for the metastable ternary phases, Ayer *et al*. [1] found the $Al_{10}Fe_2Ce$ and $Al_{10}Fe_5Ce$ phases in the similar alloys, however, these two phases were never detected and only a minor $Al_{16}Fe_3Ce$ phase was observed in our study. Determination of the lattice symmetry for the $Al_{16}Fe_3Ce$ phase is underway. For the equilibrium ternary phase, Angers [1] reported that the equilibrium ternary phase is $Al_{10}Fe_2Ce$, but Ayer *et al*. [2] pointed out that the equilibrium ternary phase should be $Al_{13}Fe_3Ce$. In our study, the equilibrium ternary phase is detected to be $Al_{13}Fe_3Ce$.

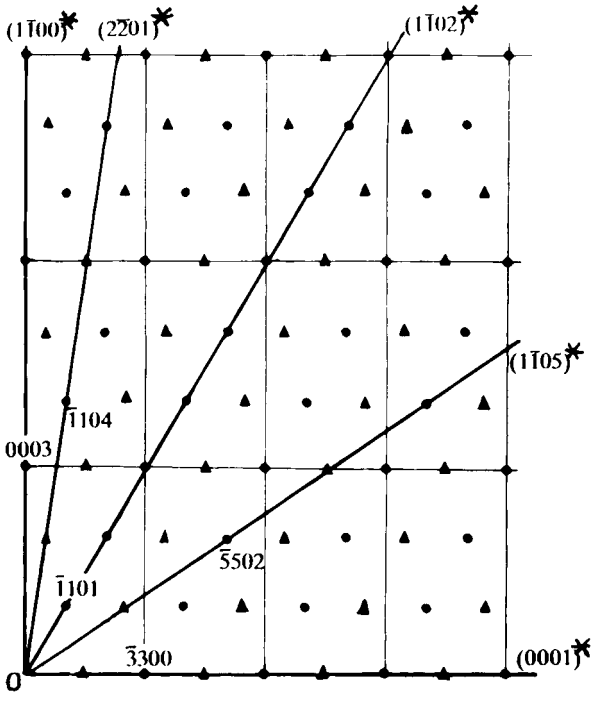

Figure 3 Projection of different DPs (thick lines) on the (11–20)* reciprocal plane of the Al_8Ce phase.

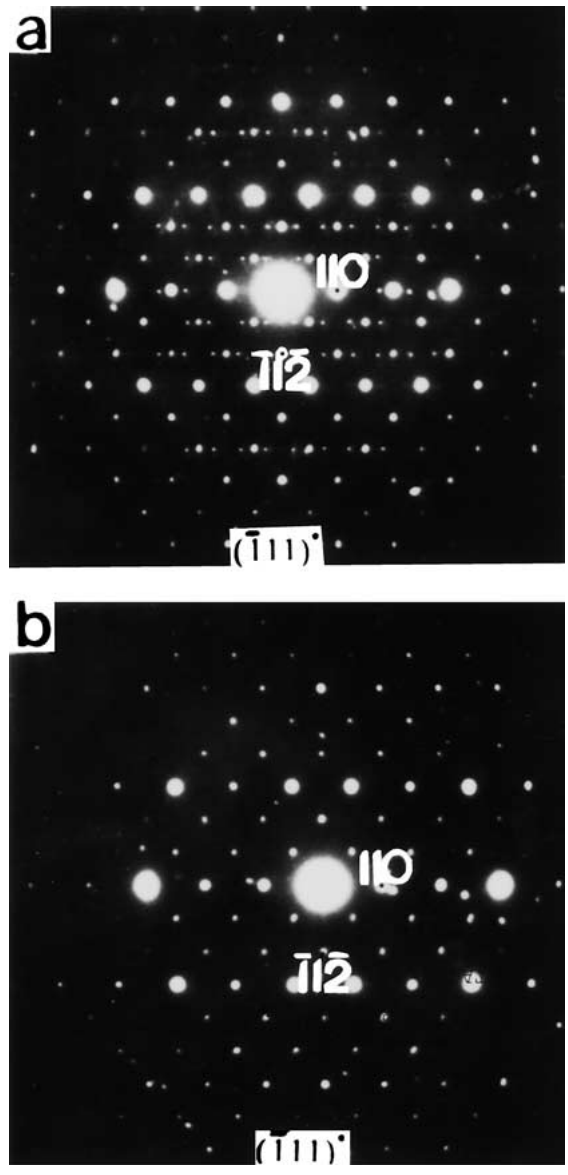

Figure 4 [100]* high-resolution TEM image of the three-fold domains in the $Al_{13}Fe_3Ce$ phase, where the (001) planes for these domains were marked.

3.2. Al_8Ce phase and $Al_{13}Fe_3Ce$

Al_8Ce phase in this Al-Fe-Ce alloy was firstly reported in our earlier work [8]. It is a metastable phase, and the atomic ratio of $Al:Ce = 8:1$ was obtained by means of energy dispersive x-ray analysis which was carried out in a JEM-200CX TEM. The structure was determined by the following process. A series of diffraction patterns (DPs) in different zone axis were obtained by tilting, as shown in Fig. 2. The tilting angles among these DPs were also displayed in the Fig. 2. Fig. 3 is the projection of DPs along the tilting axis. In Fig. 3, some thick lines represent the corresponding DPs, respectively. The symbols of solid dots and solid triangles represent the diffraction spots located at different reciprocal layers with the heights of 0 and 1/2, respectively. According to the arrangement of the solid dots and triangles, a unit cell with rhombohedral symmetry (marked by the thinner lines) could be deduced with the lattice parameters $a = 1.4$ and $c = 0.7$ nm. Correspondingly, the DPs were indexed by using this lattice symmetry and parameters (See Fig. 2), according to reflection condition $-h + k + l = 3n$ (n is integer) when the rhombohedral lattice was labeled with hexagonal coordinate system.

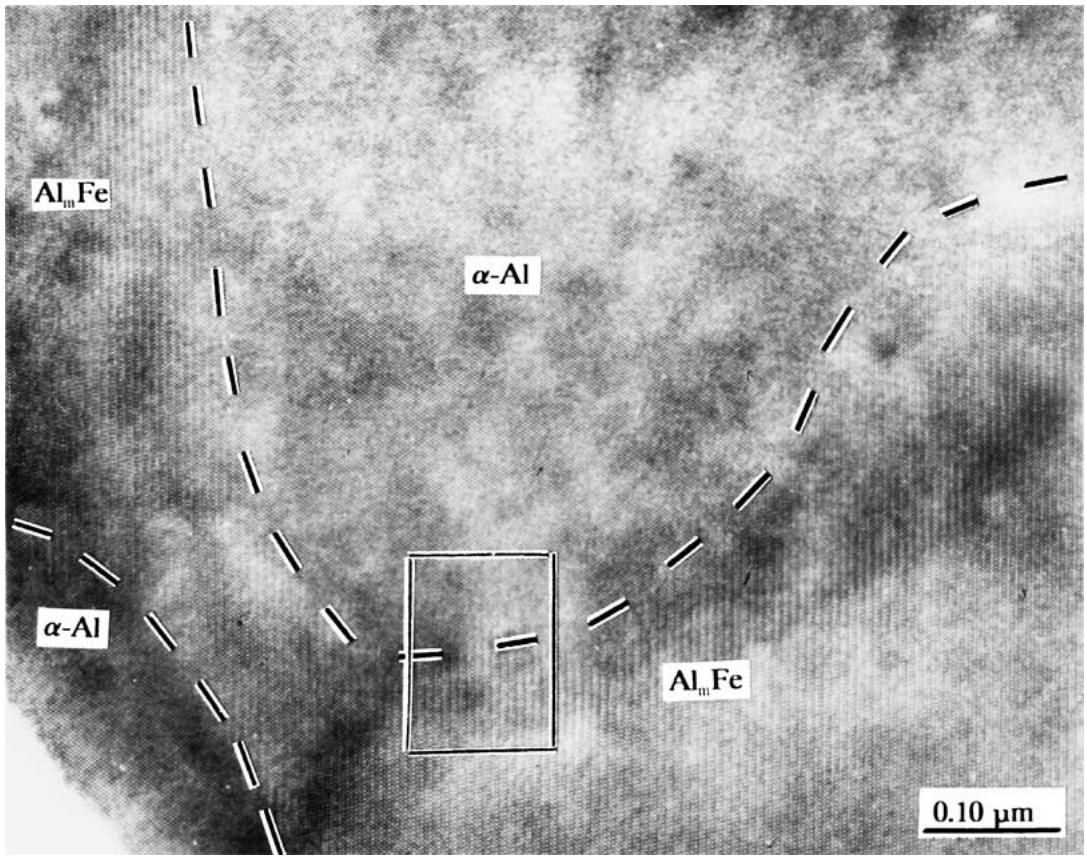

(a)

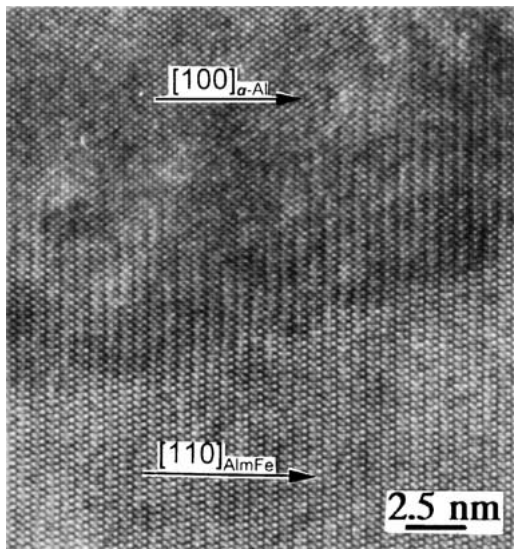

(b)

Figure 5 [100]* high-resolution TEM images of the $Al_{13}Fe_3Ce$ phase showing (a) translation domains, (b) reflection domains, and (c) translation-reflection domains.

The $Al_{13}Fe_3Ce$ phase appeared in the samples heat exposed above 315°C. This is an equilibrium phase. The equilibrium $Al_{13}Fe_3Ce$ phase belongs to a C-centered orthorhombic lattice; the possible space group is Cmcm or Cmc2 [2]. High-resolution TEM images revealed many domain structures in this phase. For example, Fig. 4 shows three-fold rotation domains. The three (001) planes in different domains are marked with black-white lines in Fig. 4. It can be seen that the three-fold domain boundaries are not quite regular, i.e., without relatively flat domain boundaries. In addition, we have also observed other kinds of domains with flat boundaries, which are shown in Fig. 5. In Fig. 5, all white rectangles represent [100] projections of one unit cell of All3Fe3Ce, and parts of the domain boundaries have been noted with black dots. According to the relative positions among these marked unit cells, we can determine that Fig. 5a–c represent translation domains, reflection domains, and translation-reflection domains, respectively.

According to the disappearance of unstable Al_8Ce and the final formation of $Al_{13}Fe_3Ce$ above 315°C (See Table I), it is reasonable to regard the $Al_{13}Fe_3Ce$ phase as a resultant of Fe diffusion into the binary Al_8Ce phase. Moreover, the three-fold domains in $Al_{13}Fe_3Ce$ imply that the equilibrium phase $Al_{13}Fe_3Ce$ be formed by phase transformation from a parent phase with three-fold symmetry, as similar to that in the Ni_3Nb phase [9]. So it is further evident that the binary Al_8Ce phase with three-fold symmetry may act as such parent phase.

3.3. Al_mFe and $Al_{13}Fe_4$

The metastable Al_mFe phase belongs to a body-center tetragonal structure with lattice parameters $a = 0.884$ and $c = 2.1$ nm [10]. Usually, the m value is ~4.0–4.4, and the size of Al_mFe becomes small with increasing

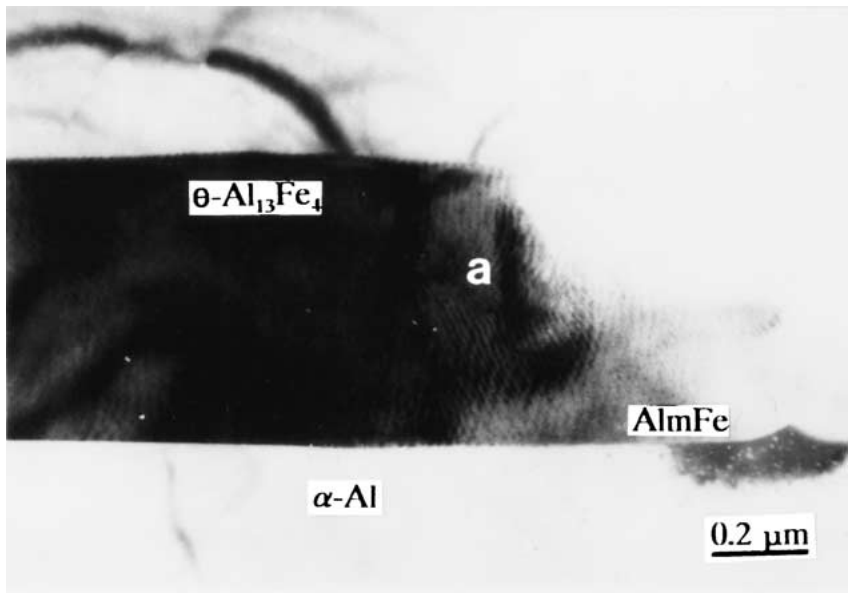

Figure 6 DPs from the Al_mFe phase showing (a) existence of satellite spots along its [110] direction and (b) disappearance of satellite spots after electron beam irradiation for a short time.

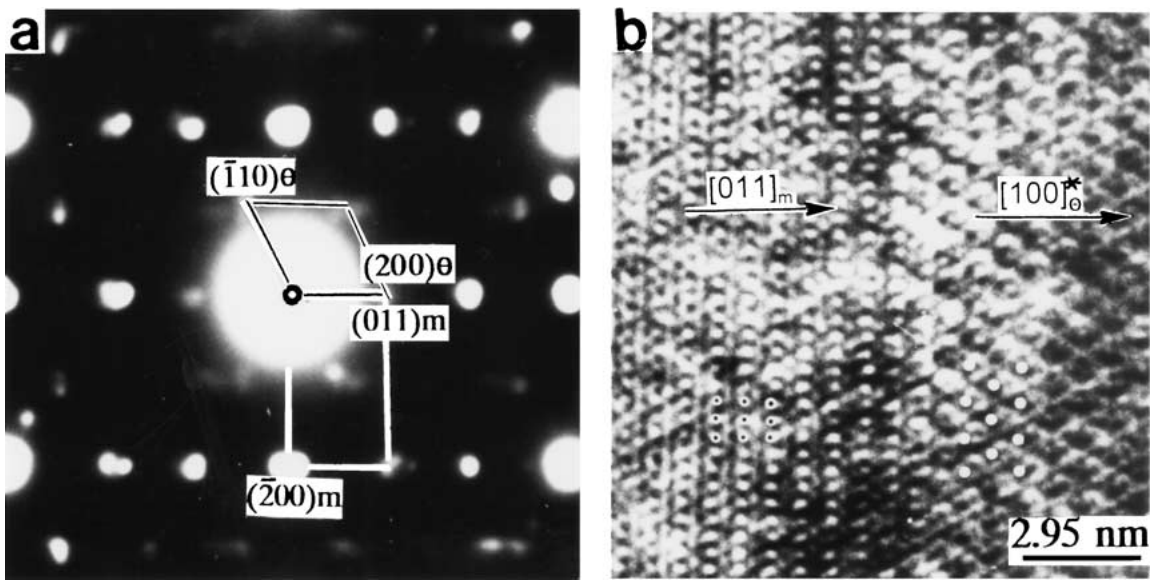

Figure 7 (a) High-resolution TEM image showing precipitation of the Al_mFe phase from α-Al solid solution and (b) an enlargement corresponding to the framework area of Fig. 7a.

the cooling rate during solidification [11]. DP in Fig. 6a from this phase shows many satellite spots along its [110] direction, suggesting numerous {110} planar defects in this phase. However, these satellite spots vanish under electron beam irradiation for a short time (seeing Fig. 6b), as supports Skjerpe's result of vacancy existence in this phase [11].

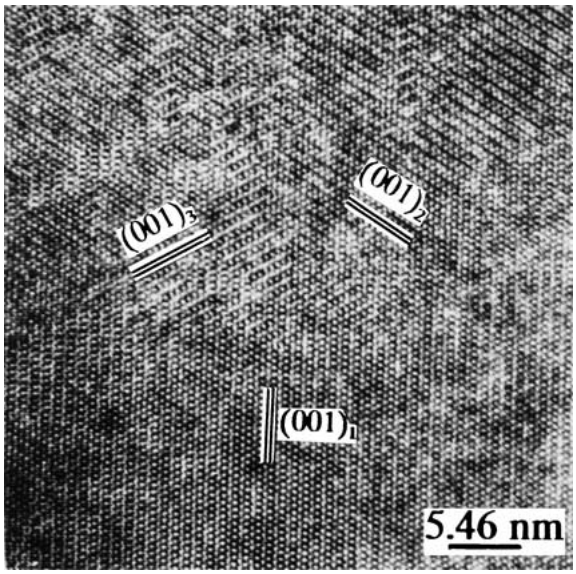

Figure 8 Bright-field. TEM image showing phase transition from Al_mFe to α-$Al_{13}Fe_4$.

Formation of Al_mFe in this alloy takes two ways: forming directly from the liquid state alloy and precipitating from the supersaturated solid solution. The former ones are usually located at grain boundaries, and the later inside α-Al solid solution. Accordingly, the effects of the Al_mFe phase could be divided into two: the part located at grain boundaries prevents the grain growth, and the other part located inside α-Al solid solution strengthens the α-Al matrix. The sizes of the former are relatively larger than the later, and the former one has not any orientation relationship with the solid solution. However, the later usually has a coherent relation between the $(200)_{\alpha\text{-Al}}$ and $(1\text{-}1\text{-}10)_{Al_mFe}$, as shown in Fig. 7a. The trace of the Al_mFe/α-Al interfaces was marked by the dashed lines. It shows that this interface is a transitional one, i.e., the interface is not very distinct. Fig. 7b, which is an enlarged image corresponding to the framework area of Fig. 7a, has further presented this interfacial feature.

The α-$Al_{13}Fe_4$ phase belongs to C-centered monoclinic with lattice parameters of $a = 1.549$, $b = 0.808$, and $c = 1.247$ nm, and $\beta = 107^\circ$ [12]. From Table I, one can see that the α-$Al_{13}Fe_4$ phase always exists in the as-extruded and all heat exposed samples. In fact, these α-$Al_{13}Fe_4$ particles result from direct formation during solidification and phase transition during heat exposure, respectively. In an as-extruded sample, the α-$Al_{13}Fe_3$ was from the liquid solidification, and most of α-$Al_{13}Fe_4$ are located at grain boundaries. However,

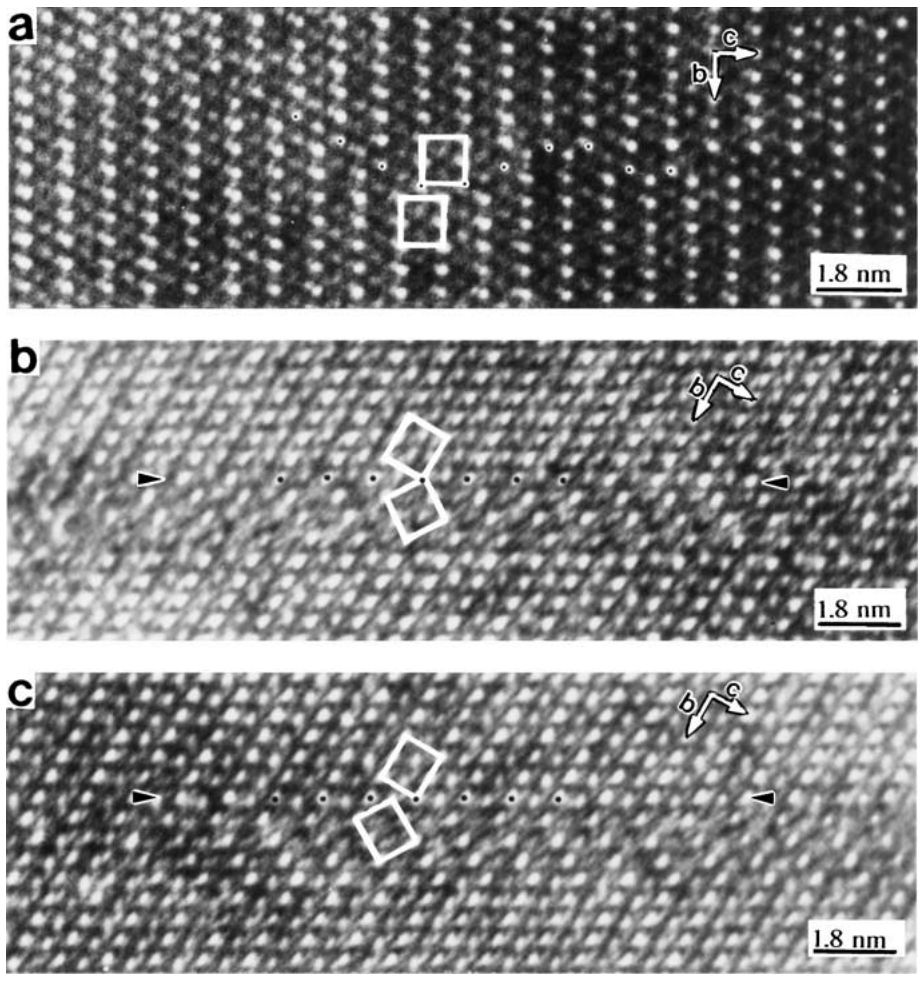

Figure 9 (a) $[01\text{-}1]_{Al_mFe}/[001]_{\alpha\text{-}Al_{13}Fe_4}$ composite DP and (b) high-resolution TEM image viewed along $[01\text{-}1]_{Al_mFe}/[001]_{\alpha\text{-}Al_{13}Fe_4}$.

the α-$Al_{13}Fe_4$ particles in the heat exposed samples consist of three parts: formation during solidification, precipitation from the α-Al supersaturated solid solution and transformation from Al_mFe. The precipitation from α-Al is due to the supersaturation of Fe element in α-Al. The phase transition from Al_mFe to α-$Al_{13}Fe_4$ is because the former is a metastable one and the later is an equilibrium phase. A typical morphology of this phase transition has been shown in Fig. 8 where the α-Al, Al_mFe and α-$Al_{13}Fe_4$ were marked in the correspondent areas, respectively. Fig. 9, high-resolution TEM image taken from the region "a" in Fig. 8, gives that the phase transformation from Al_mFe to α-$Al_{13}Fe_4$ follows such an orientation relationship: $[100]_{Al_mFe}//[010]\alpha$-$Al_{13}Fe_4$ and $(011)_{Al_mFe}//(200)\alpha$-$Al_{13}Fe_4$.

4. Conclusions

From experimental results and discussion above, we could conclude:

1. Five dispersed phases—the metastable phases, which are Al_mFe, Al_8Ce, $Al_{16}Ce_3Fe$ and the equilibrium phases α-$Al_{13}Fe_4$, $Al_{13}Fe_3Ce$, exist in the as-extruded and the heat exposed samples of the rapidly solidified Al-8.32Fe-3.4Ce(wt%) alloy. The metastable Al_mFe and Al_8Ce phases were firstly observed in the Al-Fe-Ce alloys.

2. Al_8Ce binary phase has a rhombohedral lattice with parameters of $a = 1.4$ nm, $c = 0.7$ nm. The formation of Al_mFe and Al_8Ce is related to the relatively high cooling rate during solidification.

3. Numerous rotation domains, translation domains, reflection domains and translation-reflection domains were found in the equilibrium $Al_{13}Fe_3Ce$ phase.

Acknowledgement

The project was supported by Natural Science Foundation of the Chinese Academia Sinica, which is acknowledged.

References

1. L. ANGERS, *Diss. Abstr. Int.* **46** (1986) 288.
2. R. AYER, *Metall. Trans.* **19A** (1988) 1645.
3. B. GRLEB, *Bulletin of Alloy Phase Programs* **10** (1989) 669.
4. H. JONES, *Mater. Sci. and Eng.* **5** (1969/1970) 1.
5. C. HUANG, L. C. ZHANG, A. Q. HE, Q. Y. CHEN, Y. C. ZHANG and H. Q. YE, *Transactions of Nonferrous Metals Society of China* **5** (1995) 82.
6. P. SKJERPE, *Metall. Trans.* **18A** (1987) 189.
7. R. M. K. YOUNG and T. W. CLYNE, *Scripta Metall.* **15** (1981) 1211.
8. L. C. ZHANG, A. Q. HE, H. Q. YE, Y. C. ZHANG and C. HUANG, *Acta Metallurgica Sinica* **31** (1995) 519.
9. J. P. ZHANG, H. Q. YE, K. H. KUO and S. AMELINCKX, *Phys. Status Solidi* **93A** (1986) 437.
10. H. KOSUGE and I. MIZUKAMI, *J. Jpn. Inst. Light Metals* **25** (1975) 1.
11. P. SKIERPE, *Acta Cryst.* **44B** (1988) 480.
12. P. J. BLANK, *ibid.* **8A** (1955) 43.

Received 26 March
and accepted 9 September 2002